

MULTI-LASER POWDER BED FUSION OF CU10SN USING LOW-POWER 450NM DIODE LASERS

E. Cetin^{1,2}, A. Aydin¹, S. C. Erman¹, K. Mumtaz^{1,*}

¹ Department of Mechanical Engineering, The University of Sheffield, Sheffield, United Kingdom, S14BJ

² Department of Mechanical Engineering, Hitit University, Çorum, 19030, Türkiye

*Corresponding author: k.mumtaz@sheffield.ac.uk

Abstract

Due to its inherent high reflectivity, the processing of copper and its alloys is challenging using low power lasers. Literature reviews indicate that using a 450 nm blue laser for processing copper increases absorptivity dramatically from 5% to 65% (x13 higher) compared to traditional laser powder bed fusion (LPBF). Therefore, this study aims to demonstrate that diode lasers with a wavelength of 450 nm are suitable for producing Cu10Sn samples. In this work, diode point melting additive manufacturing technique was used and single layers were produced using diode lasers connected to the X-Y portal to scan on the copper substrate. Various hatch distances (i.e., 50, 75, 100, and 125 μm), scanning speeds (ranging from 150 to 2100 mm/min), and laser powers (20 and 40 W) were selected as process parameters. To determine the mechanical and physical properties of the sample, surface roughness, relative density and melt pool characterization were examined. The results showed that the surface roughness value of samples produced with low hatch distance and low scanning speeds (i.e., in high surface energy values) for 20 W laser power is approximately up to 3.5 times lower than that of 40 W laser power. Additionally, optical analysis of the top surface images revealed that the surface energy density values of Cu10Sn samples with a relative density of 85% or higher ranged between 22 and 30 J/mm². Furthermore, the highest relative density value was found to be 87.84% with laser power of 40 W, hatch distance of 50 μm , and scanning speed of 2100 mm/min.

Keywords: Additive Manufacturing, Cu10Sn, Diode Point Melting (DPM), blue lasers

1. Introduction

Additive manufacturing emerges as an innovative alternative to traditional production methods, offering the ability to easily produce complex geometries and minimize material waste. Various additive manufacturing techniques include powder bed fusion [1], binder jetting [2], material extrusion [3], vat polymerization [4], material jetting [5], and energy deposition [6]. Among them, powder bed fusion technology is frequently used in many industrial fields due to its advantages such as high resolution, wide material compatibility, material efficiency, superior mechanical properties and ease of post-production processing compared to other additive manufacturing methods [7,8].

LPBF metal additive manufacturing technologies such as direct metal laser sintering (DMLS) and selective laser melting (SLM) are increasingly being used in the automotive, aerospace, and energy sectors to produce high-value end-use components. High power fiber lasers (usually 200–1000 W) are used in LPBF processes to create a focused, high energy density laser spot (40–100 μm diameter) that melts portions of a thin layer of metallic powder feedstock that has been pre-deposited layer by layer. With this technology, a single high power

fiber laser module [9] or multiple lasers [10] are deflected across the powder bed using a mechanically guided galvanometer (galvo) mirror to selectively melt sections of the powder bed based on sliced 3D CAD data. This technology processes nearly full density parts from various engineering metals or metal alloys such as aluminum [11], titanium [12], steel [13] and nickel [14].

Copper and its alloys are extensively used in industries such as aerospace, electronics, and construction due to their remarkable electrical and thermal conductivity, high corrosion resistance, and cost-effectiveness [15]. Nevertheless, the high thermal conductivity and ductility of Cu pose challenges for conventional manufacturing techniques, including machining and welding. Consequently, existing manufacturing practices are limited to producing basic geometries such as wires, bars, and sheets, which are subsequently assembled into the final product. This extensive process leads to heightened complexity and costs. With the rising demand for additive manufacturing (AM) techniques to produce complex Cu parts, numerous studies have been conducted to address this challenge. Oropeza et al. [16] investigated the processing of copper, bronze, and brass samples to establish the necessary correlation between powder bed fusion parameters, resultant porosity, and material properties. Liu et al. [17] employed laser powder bed fusion (L-PBF) additive manufacturing to produce high-strength copper (Cu) alloys by introducing cobalt (Co) submicron particles into pure Cu powder through inoculation.

The use of copper and copper alloys in LPBF processes has some drawbacks because of the nature of copper such as high laser beam reflectivity, high thermal conductivity and high bonding tendency towards oxygen [18]. The primary challenge in the processability of copper arises from its poor laser absorption rate, which is potentially just 2-6% of the incident energy when exposed to Yb-fiber lasers with a wavelength of approximately 1064 nm [19]. Furthermore, the temperature distribution is critical to the stability of the SLM processing of pure Cu since copper's optical absorption depends on both the temperature of the material and the wavelength of the incoming radiation [20]. Copper has a mean absorptance rate in the near-infrared region of less than 6% at room temperature, which is significantly less than that of other metallic alloys. The absorptivity increases slightly near the melting temperature [21]. Low laser absorption and strong thermal conductivity both lower the energy needed to melt the material and create a stable melt pool. Another fundamental problem caused by this high reflection is the damage that the reflection may cause to the optical mirror. To overcome the above-mentioned problems, lower wavelengths such as blue and green lasers have been proposed in the literature [22–26]. Limited approval of LPBF Cu prior art, it was essential to determine the process parameters. Therefore, in this study, various process parameters were focused on single layer Cu10Sn samples, and briefly discussed. In this context, different hatch distances, scanning speed and laser power values were chosen as process parameters.

2. Experimental methodology

2.1. Powder material

As can be seen from Figure 1, copper alloy, which is very difficult to produce with high wavelength lasers due to its high reflectivity, was chosen in this study. The study employed blue lasers with a wavelength of 450 nm and utilized Cu10Sn powder as the material. The Cu10Sn powder used in this study were supplied by Makin Metal Powders Ltd. The chemical composition of Cu10Sn is given in Table 1.

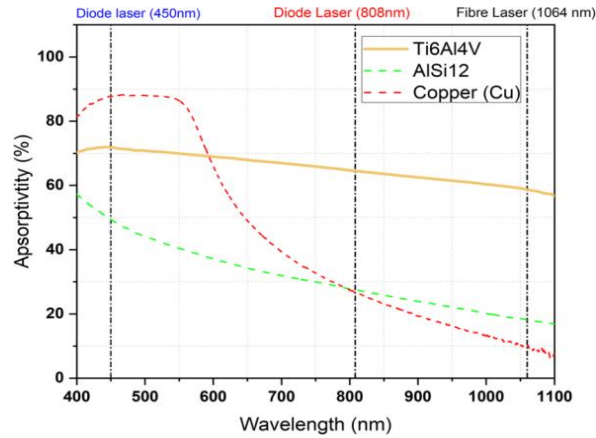


Figure 1. The optical absorption of Cu, AlSi12, and Ti6Al4V between 400 and 1100 nm in wavelength [27]

Table 1. Chemical composition of the Cu10Sn [28]

Material	Chemical compositions (wt%)		
	Cu	Sn	P
Cu10Sn	Balance	9.2-11.0	0.10 - 0.35x

2.2. System operating procedures

In this study, it was aimed to reveal that copper samples with very low absorbance can be produced by using low-wavelength diode lasers as an alternative to techniques such as high-wavelength SLM. In this context, optimum scanning speed, hatch distance and laser power were obtained by performing a single layer study. Hatch distance with 25 μm different intervals from 50 to 125 μm , scanning speed with 150 mm/min intervals from 150 to 2100 mm/min, and two different laser power production parameters, 20 and 40W, were taken into account. The experimental design used in this study is presented in Figure 2. The one-way zigzag scanning strategy was chosen as the scanning approach. A total of eighty-four different square samples ($4 \times 4 \text{ mm}^2$) were produced for each case.

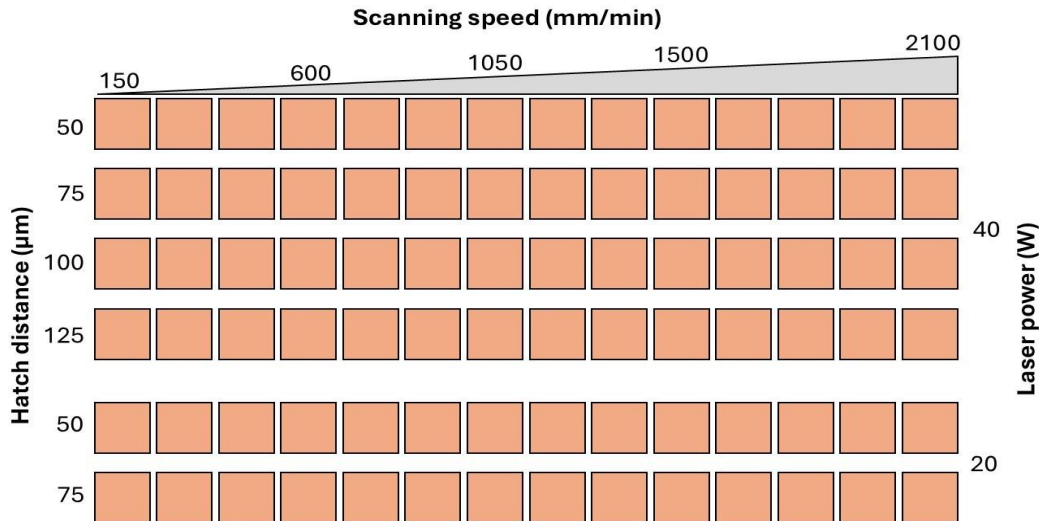


Figure 2. Experimental design used in this study.

The diode point melting technique, which includes orientation and focusing lenses, was used to obtain localized melting within the desired area. This production technique is a technique in which 8 different 450 nm blue diode lasers can produce by focusing on a single point. The laser holder and a gantry system were housed in a closed chamber with powder bed pistons. The diode point melting machine used in this study is shown in Figure 3. Before the process started, the chamber was purged with argon gas until the oxygen level in the chamber was below 0.1%, and it was checked with an oxygen sensor to ensure that the oxygen level did not to increase throughout the process. A wiper blade spreads the Cu10Sn powder uniformly on the substrate in the production area.

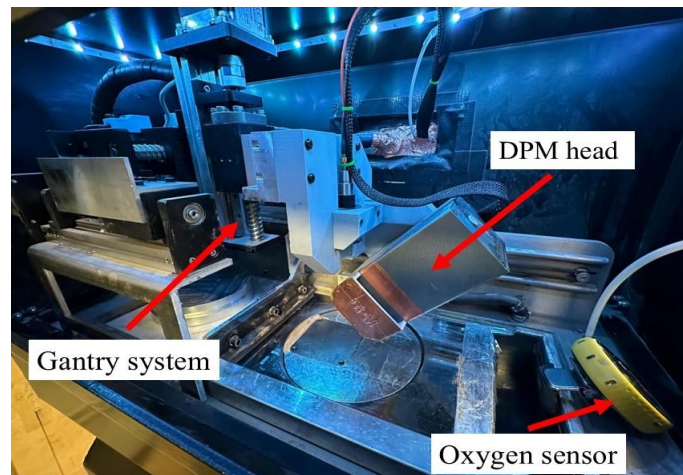


Figure 3. The diode point melting machine used in this study

2.3. Measurement Methods

In this study, the surface roughness, relative density and melt pool characterization of the samples produced with different hatch distance, scanning speed and laser power were examined. Surface roughness is a measure of the texture of a surface and quantifies its irregularities. Key parameters used to evaluate surface roughness include Ra, Rq, and Rz. These parameters provide critical information about the roughness and profile characteristics of the surface. Only the Ra value was used in this study, and the formula for the Ra value is as follows.

$$Ra = \frac{1}{L} \int_0^L |Z(x)| dx \quad (1)$$

where L is the sampling length and $Z(x)$ is the height of the profile at position x . The top surface roughness of the produced samples was examined optically using Alicona Infinite Focus SL. Additionally, an optical microscope under 5x magnification was used to determine relative density and melt pool examination. For the microscopic examination, the specimens were mounted in bakelite using a Buehler Simplimet Mounting Press. Following mounting, grinding and polishing were carried out with a Buehler Automet machine, utilizing 60, 320, 600, 1200, 2400, and 4000 grit papers sequentially for the grinding process. A 1 μm colloidal suspension solution was used for polishing. Before optical microscopy, the samples were rinsed with water in the Automet machine and cleaned with isopropanol. A Nikon optical microscope was employed to capture the density maps, and ImageJ software was used to determine the density results. This image correlation software significantly reduced calculation time compared to the Archimedes method, especially when handling multiple samples, by consistently using the same threshold values to ensure more accurate results. Relative density determination was carried out from the top surface of the samples and melt pool characterization was examined from the cross-sectional area. The relative density values were found using the

images obtained on the optical microscope with the image analysis technique. Although the results obtained from samples produced with a single layer do not represent an actual sample, since it is the first study in which copper samples were examined with blue diode lasers, surface energy density was used instead of volumetric energy density in this study. The surface energy density (E_s) formula used in the literature was also used to evaluate the effect of hatch distance scanning speed and laser power on surface roughness and relative density. The E_s formula is defined as

$$E_s = \frac{P}{s \times h} \quad (2)$$

where P , s and h are the laser power, scanning speed and hatch distance.

3. Results and Discussion

3.1. Relative density and defects of the single layer of Cu10Sn samples

Upon reviewing literature studies on samples produced using LBPF methods, it is commonly observed that there are three types of defects. These are the keyhole mechanism caused by low scanning speed and excessive energy density, the balling mechanism that can occur at high speed and high laser power, and the lack of fusion mechanism caused by insufficient low power and high speed. Figure 4 shows the images of Cu10Sn samples produced at 40W and having a hatch of 100 μm . As can be seen from the figure, examining the top surfaces of the Cu10Sn samples, it was observed that certain regions contained pores, while other regions contained sintered powders that were not completely melted (partial melting). The pores were formed due to excessive energy density, especially at very low scanning speeds (e.g., 150 mm/min). This is because the copper alloy that was chosen has a very high conductivity. In addition, it has been observed that in some cases of high speed and low laser power, there is no complete melting in some regions and the powder is only sintered. The top surface images of Cu10Sn alloy samples produced with a 40W laser for different scanning speeds are presented in Figure 5.

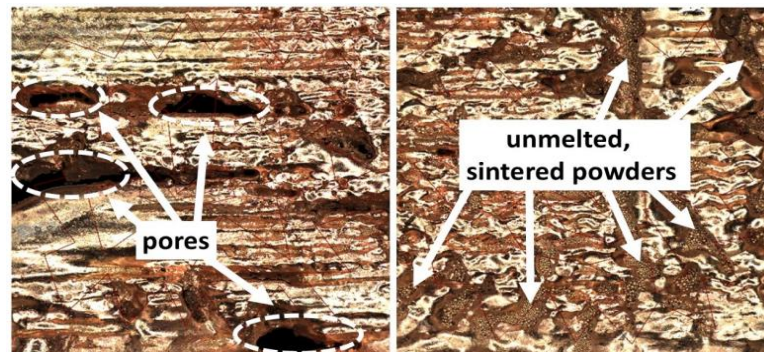


Figure 4. The defects of Cu10Sn alloy samples produced with laser of 40W.

Upon examining Figure 5, it is evident that there are numerous sintered particles that have not undergone melting. However, for the same hatch distance values, as the speed increases, an improvement in the top surfaces of the structures is noticeable. For example, in samples with a hatch value of 50 μm , there are many unmelted but sintered powders at a scanning speed of 300 mm/min, while a much smoother surface is seen at a scanning speed of 2100 mm/min. Similar situations were observed in samples with different hatch values. Relative density values were determined by the image analysis method using the top surface images in Figure 5 and are presented in Figure 6.

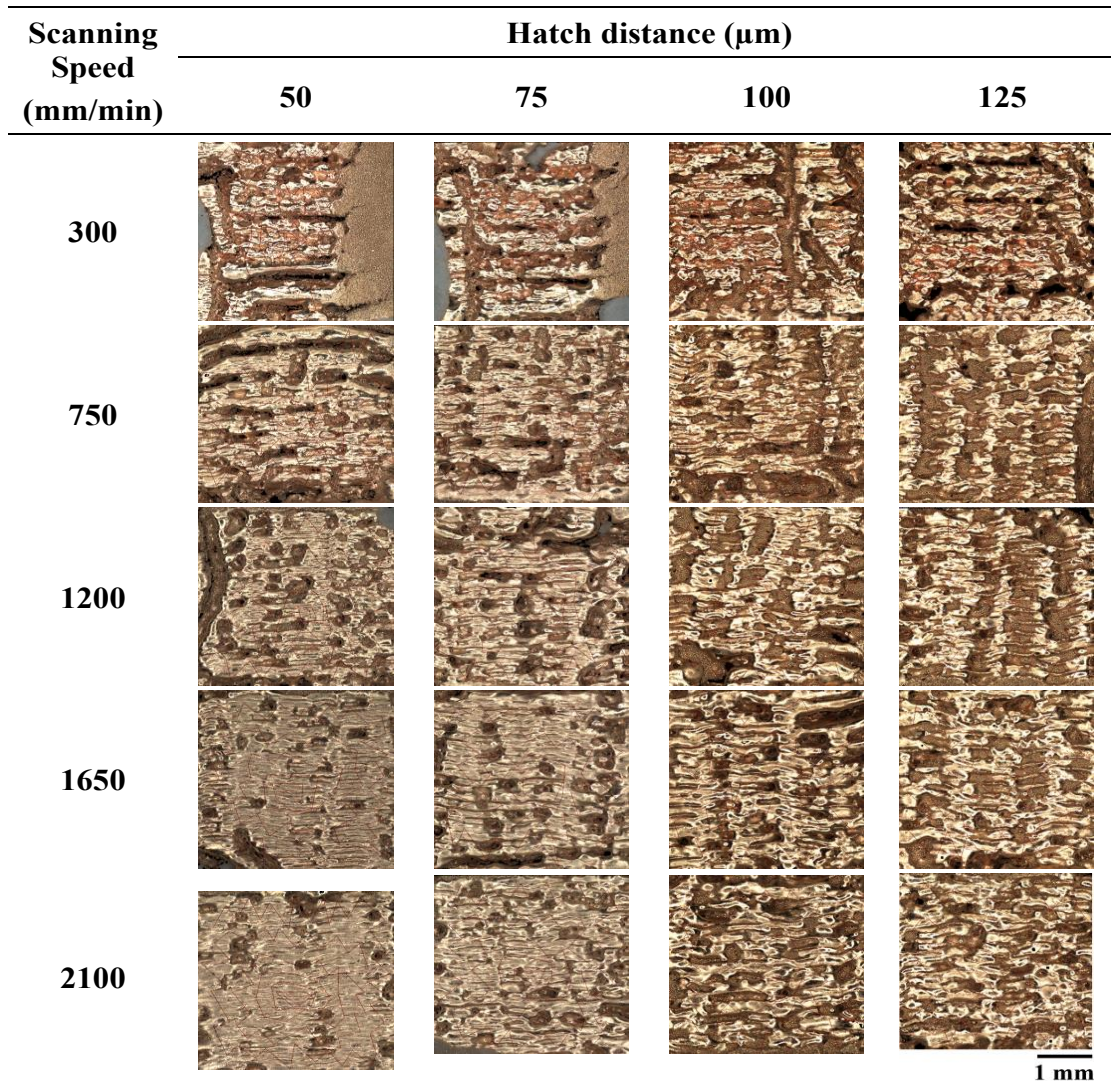


Figure 5. Top surface images of Cu10Sn alloy samples produced with laser of 40W for different scanning speeds.

While Figure 4a contains relative density values according to different speed values, Figure 4b contains relative density values according to different surface energy density values. Considering the 50 μm hatch value, it is seen that the density values vary between approximately 65% and 88%. At scanning speed values of 150 and 300 mm/min, together with the high surface energy density value, excessive energy is applied to the material and as a result, visible separations are observed in the material. As a result, obvious complete opening or partial pores are formed on the sample, and therefore the relative density of the sample is low. It is also seen that as the scanning speed value increases, the relative density value also increases. Considering Equation (2), as seen in Figure 3 and Figure 4a, for constant laser power, the surface energy density value decreases as the hatch distance or scanning speed increases. Therefore, it has been observed that relative density values are better at high scanning speeds, that is, in scenarios where surface energy density values are lower. It is seen that the surface energy density values of samples with high relative density (higher than 86%) are between 22-25 J/mm^2 . On the other hand, it can be seen that the structures with the lowest density (approximately 65%) are the samples with the highest surface energy density values (160 and 320 J/mm^2).

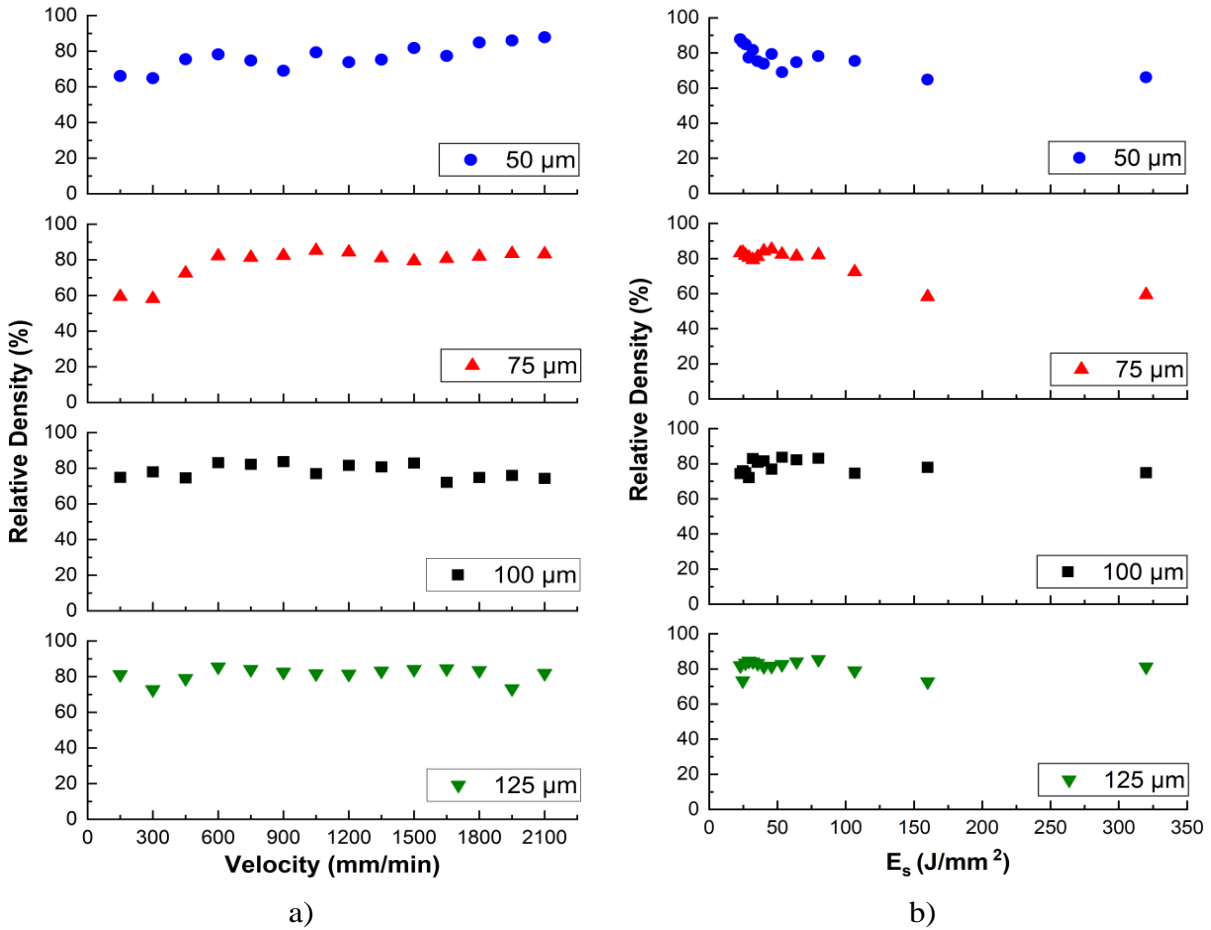


Figure 6. Relative density values of Cu10Sn alloy samples produced with laser of 40W for a) different scanning speeds and b) surface energy density values.

Similar situations also apply to samples with a hatch value of 75 μm. It was observed that the structures with the highest relative density among the samples with 75 μm hatch value were the samples with scanning speeds of 1050 and 1200 mm/min and surface energy density values of 26.67 and 30.48 J/mm², respectively. However, similar to the samples with a hatch value of 50 μm, the lowest density samples were observed in the samples with the lowest scanning speed. The surface energy density values of these samples, which have relative density values of 58.21% and 59.38%, were calculated as 213.33 and 106.67 J/mm², respectively. In the samples with 100 μm hatch value, it was observed that the samples with the highest relative density values (83.70% and 83.13%) were the samples with 26.67 and 40 J/mm² surface energy density values. On the other hand, the samples with the lowest relative density values (72.12% and 74.35%) were found in samples with surprisingly high speeds and therefore very low surface energy density values (14.55 and 11.43 J/mm², respectively). When the samples with 125 μm hatch distance value were examined, it was seen that the samples with the highest density were those with 84.48% (11.64 J/mm²) and 85.45% (32.0 J/mm²) relative density. However, the lowest density samples, with relative densities of 72.73% and 73.27%, had surface energy densities of 64.0 J/mm² and 9.85 J/mm², respectively, similar to those with a hatch value of 100 μm.

Considering the relative density results of Cu10Sn samples with different hatch and scanning speed values, it was determined that the surface energy density values of the samples

with a relative density of 85% and above were between 22 and 32 J/mm². On the other hand, the results also clearly revealed that although the surface energy density value is an important indicator, it is not the only one that is adequate.

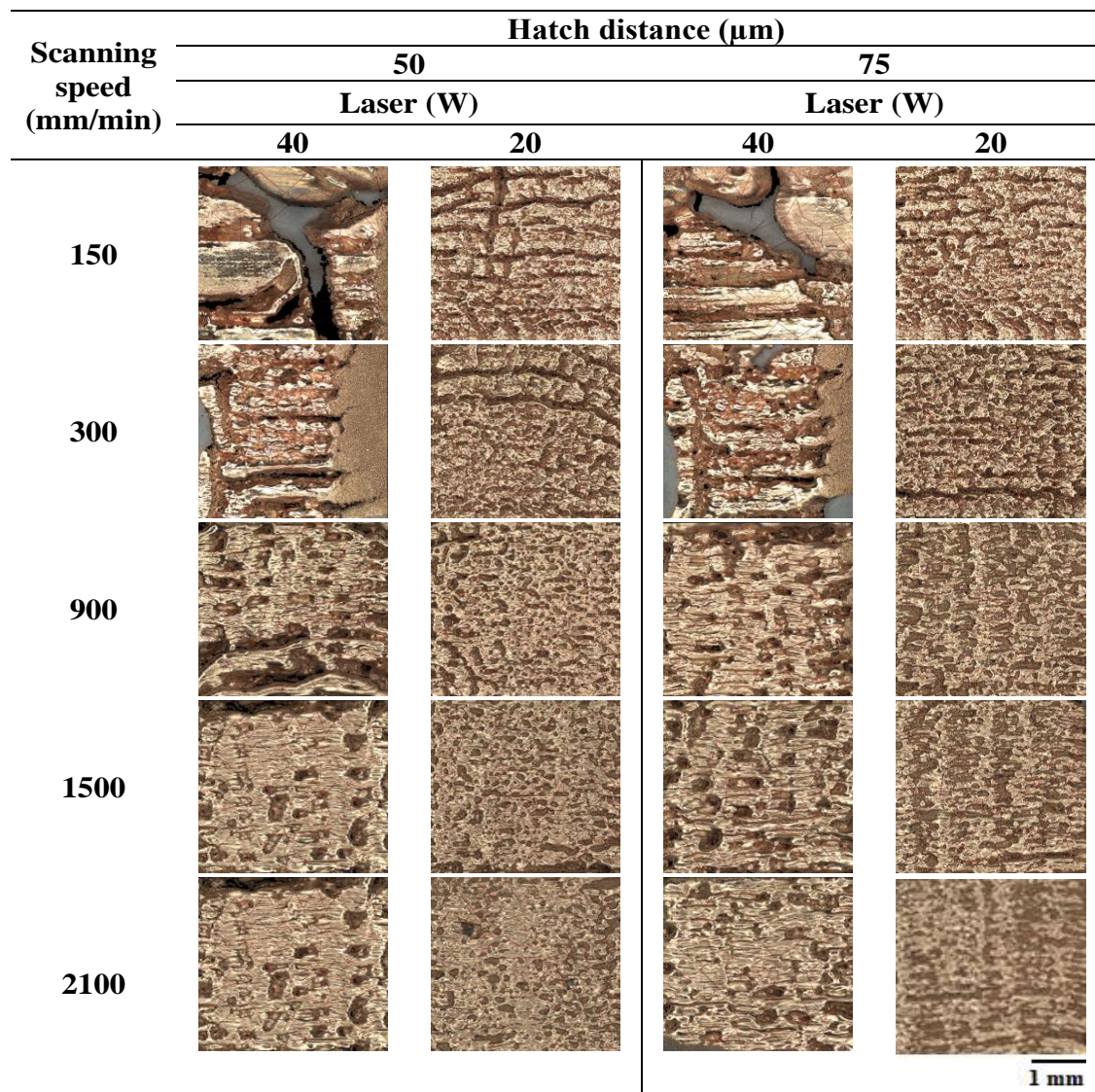


Figure 7. Top surface images comparison of Cu10Sn alloy samples produced with laser of 40W and 20 W for different scanning speeds.

In the previous lines, the relativity densities and defects of the samples produced with 40 W laser power were discussed. In the examinations, it was observed that the samples taken at 40 W laser power and very low scanning speeds had a significant number of pores due to high surface energy density values. Therefore, experimental designs with 50 and 75 μm hatch distance values, which generally have high relative densities, were produced using half laser power (i.e., 20 W) and compared with 40 W ones. Top surface images and relative density comparison of Cu10Sn samples produced with laser of 40W and 20 W for different scanning speeds are presented in Figure 7 and Figure 8, respectively. When the laser power was reduced from 40 W to 20 W, the size and number of defects on the top surface decreased significantly, as can be clearly seen in Figure 7. This situation is more clearly understood in the graphs in Figure 8. In Figure 8, reducing the laser power, especially at low speeds such as 150, 300 and

450 mm/min, had a positive effect in terms of relative density. In particular, for 50 μm hatch value, the relative density values of the samples produced with 40W laser power and 150, 300 and 450 mm/min scanning speeds were 66.10%, 64.84% and 75.48%, while those produced with 20 W laser power were calculated as 80.98%, 82.67% and 81.73%, respectively. After 1500 mm/min scanning speed, it is seen that the relative density values of the samples produced with 20 and 40W laser powers are similar.

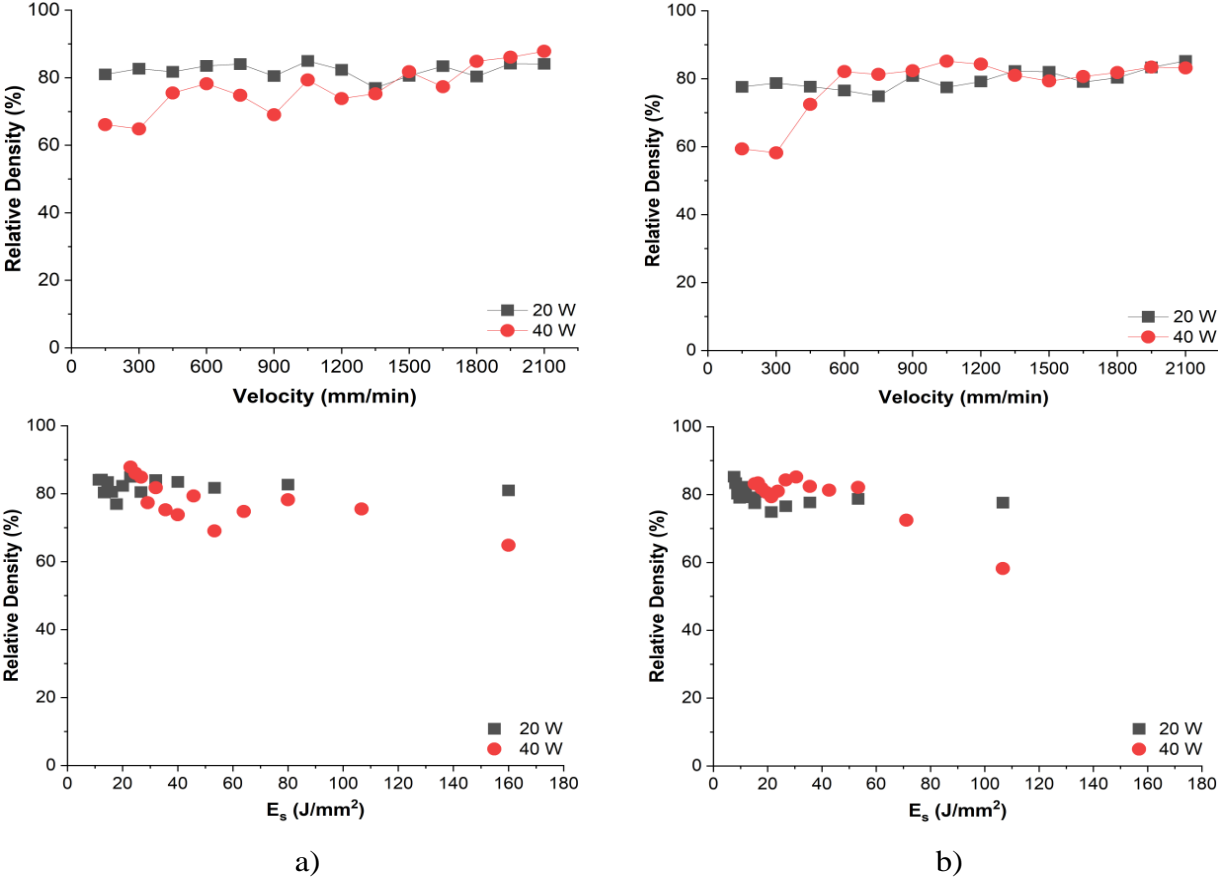


Figure 8. Relative density comparison of Cu10Sn alloy samples produced with laser of 40W and 20 W and hatch distance of a) 50 μm and b) 75 μm for different scanning speeds and surface energy density values.

In addition, for the 50 μm hatch distance, the highest relative density value was found with 87.84% at 40 W laser power and 2100 mm/min scanning speed, while for 20 W laser power, the highest relative density value was found with 84.96% at 1050 mm/min scanning speed. Similarly, in samples with 75 μm hatch distance values, it is seen that the relative density values of samples with high laser power at low speeds such as 150, 300 and 450 mm/min are lower than those with low laser power. Relatively similar relative density values were found after 4500 mm/min scanning speed values for 20 and 40W laser power values. Additionally, for the 75 μm hatch distance, the highest relative density value was found with 85.27% at 20 W laser power and 2100 mm/min scanning speed, while for 40 W laser power, the highest relative density value was found with 84.30% at 1200 mm/min scanning speed. When the correlation between surface energy density values and relative density values is examined, it is seen that the highest relative density values (above 84%) vary between 7.62 and 32 J/mm^2 for both 50 and 75 μm hatch distance values. It is also seen that as the surface energy density values

increase, the surface energy density values of Cu10Sn samples decrease for both 20 and 40 W laser power values.

3.2. Surface roughness of the single layer of Cu10Sn samples

The surface roughness of a part may directly affect its functionality. For example, the smoother the surfaces of moving parts, the less friction and wear, which extends the life of the parts and improves their performance. Therefore, in this study, it was aimed to have the surface roughness as low as possible. Figure 9 shows the top surface roughness of some selected Cu10Sn samples with different scanning speed and hatch values for 40W laser power.

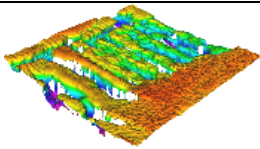
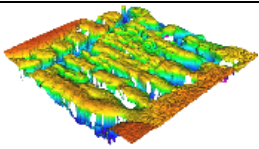
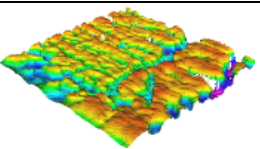
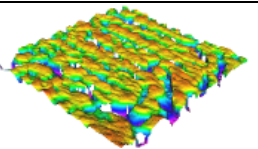
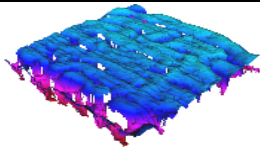
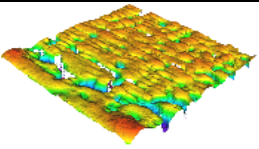
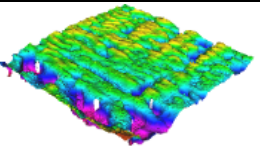
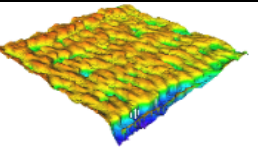
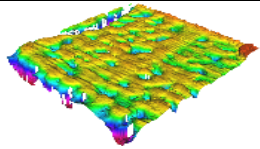
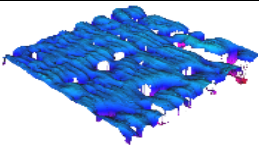
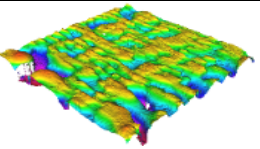
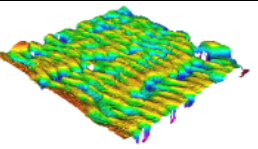
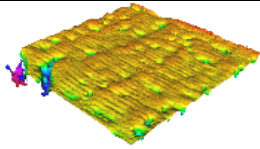
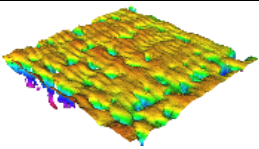
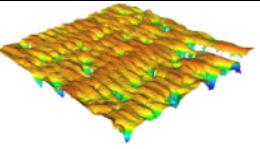
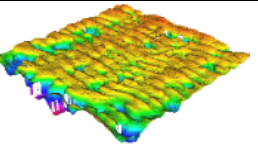
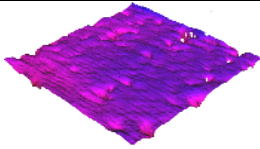
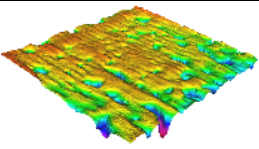
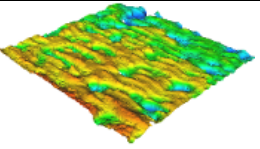
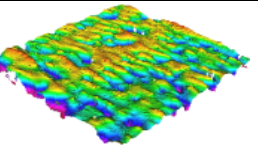
Scanning Speed (mm/min)	Hatch distance (μm)			
	50	75	100	125
300	 Ra= 83.357 μm Es= 160.00 J/mm ²	 Ra= 64.342 μm Es= 106.67 J/mm ²	 Ra= 54.151 μm Es= 80.00 J/mm ²	 Ra= 47.346 μm Es= 64.00 J/mm ²
750	 Ra= 64.244 μm Es= 64.00 J/mm ²	 Ra= 54.697 μm Es= 42.67 J/mm ²	 Ra= 53.186 μm Es= 32.00 J/mm ²	 Ra= 35.984 μm Es= 25.60 J/mm ²
1200	 Ra= 28.961 μm Es= 40.00 J/mm ²	 Ra= 51.619 μm Es= 26.67 J/mm ²	 Ra= 48.523 μm Es= 20.00 J/mm ²	 Ra= 44.443 μm Es= 16.00 J/mm ²
1650	 Ra= 16.298 μm Es= 29.09 J/mm ²	 Ra= 37.807 μm Es= 19.39 J/mm ²	 Ra= 40.921 μm Es= 14.55 J/mm ²	 Ra= 38.721 μm Es= 11.64 J/mm ²
2100	 Ra= 17.761 μm Es= 22.86 J/mm ²	 Ra= 24.094 μm Es= 15.24 J/mm ²	 Ra= 31.017 μm Es= 11.43 J/mm ²	 Ra= 39.611 μm Es= 9.14 J/mm ²

Figure 9. Surface roughness of Cu10Sn alloy samples produced with laser of 40W for different scanning speeds.

According to the figure, it can be seen that the surface roughness values vary between 16 and 83 μm . For 50, 75 and 100 μm hatch distance values, surface roughness values generally decrease as scanning speed increases. For example, for a hatch depth of 50 μm , the surface roughness value is 83.357 μm at a scanning speed of 300 mm/min, while it is 28.91 μm at a scanning speed of 1200 mm/min and 17.761 μm at a scanning speed of 2100 mm/min. Similarly, for a hatch value of 75 μm , the surface roughness value is 64.342 μm at a scanning speed of 300 mm/min, while it is 51.619 μm at a scanning speed of 1200 mm/min and 24.094 μm at a scanning speed of 2100 mm/min.

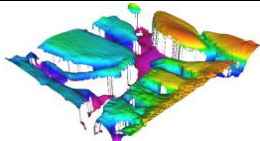
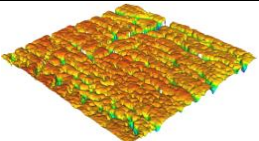
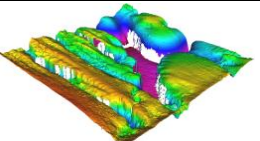
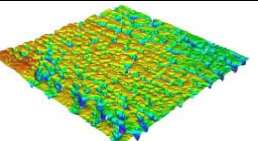
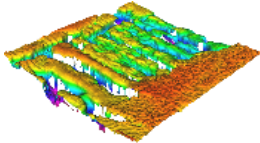
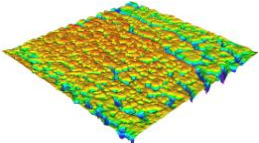
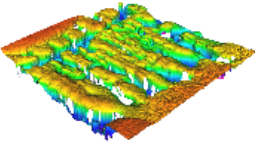
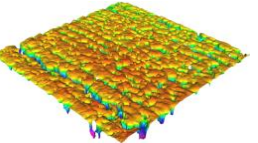
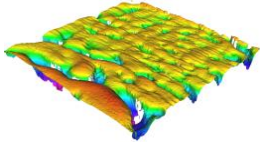
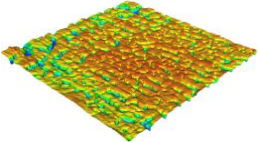
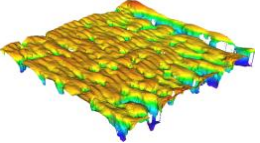
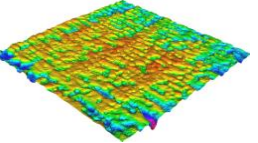
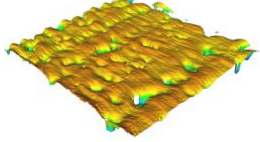
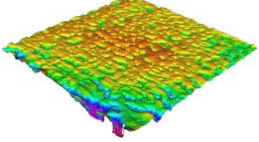
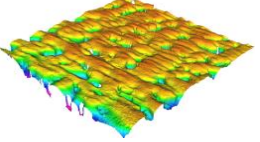
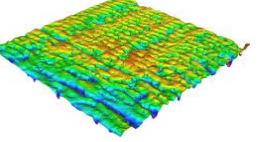
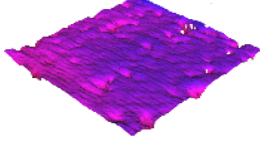
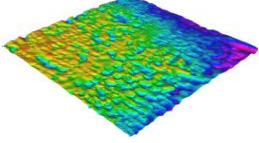
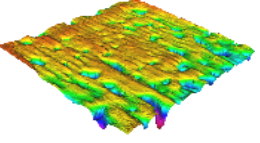
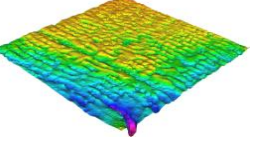
Scanning Speed (mm/min)	Hatch distance (μm)			
	50		75	
	Laser (W)		Laser (W)	
	40	20	40	20
150	 Ra= 127.062 μm Es= 320.00 J/mm ²	 Ra= 36.300 μm Es= 160.00 J/mm ²	 Ra= 105.289 μm Es= 213.33 J/mm ²	 Ra= 32.724 μm Es= 106.67 J/mm ²
300	 Ra= 83.357 μm Es= 160.00 J/mm ²	 Ra= 24.526 μm Es= 80.00 J/mm ²	 Ra= 64.342 μm Es= 106.67 J/mm ²	 Ra= 30.104 μm Es= 53.33 J/mm ²
900	 Ra= 76.476 μm Es= 53.33 J/mm ²	 Ra= 18.288 μm Es= 26.67 J/mm ²	 Ra= 48.453 μm Es= 35.56 J/mm ²	 Ra= 17.428 μm Es= 17.78 J/mm ²
1500	 Ra= 22.310 μm Es= 32.00 J/mm ²	 Ra= 14.971 μm Es= 16.00 J/mm ²	 Ra= 37.394 μm Es= 21.33 J/mm ²	 Ra= 18.869 μm Es= 10.67 J/mm ²
2100	 Ra= 17.761 μm Es= 22.86 J/mm ²	 Ra= 12.640 μm Es= 11.43 J/mm ²	 Ra= 24.094 μm Es= 15.24 J/mm ²	 Ra= 15.066 μm Es= 7.62 J/mm ²

Figure 10. Surface roughness comparison of Cu10Sn alloy samples produced with laser of 40W and 20 W for different scanning speeds.

On the other hand, at the 125 μm hatch distance value, there is no significant correlation between sample speed and surface roughness. In addition, in parallel with the relative density values, it was observed that the structures with the highest surface roughness values were the low-speed samples with the highest surface energy density, while the samples with the lowest surface roughness values were in the samples with generally low surface energy density. Figure 10 shows some selected surface roughness images of Cu10sn samples with different laser powers for different scanning speed values. As can be seen in the figure, decreasing the laser power from 40 W to 20W, in other words, reducing the surface energy density values by half, resulted in an improvement in the surface roughness values of all samples. Particularly for very low scanning speed values, halving the laser power resulted in significant improvements in surface roughness values. In particular, for 50 μm hatch distance and 150 mm/min scanning speed, the surface roughness value of the sample with 20 W laser power is approximately 3.5 times less than that of the 40 W one. This value is approximately 3.2 times for the 75 μm hatch distance value.

3.3. Melt pool characteristics of the Cu10Sn samples

Figure 11 shows some selected optical microscopy images from cross-sections of single layer Cu10Sn samples produced with a laser power of 40 W for different scanning speeds and hatch distances.


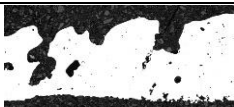





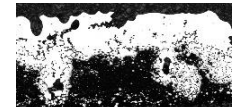
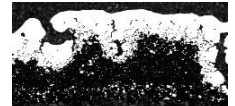
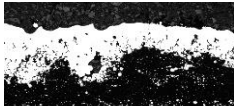
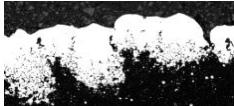

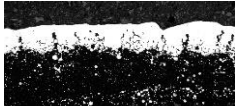
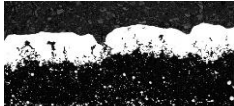
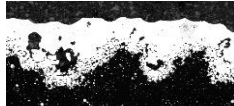
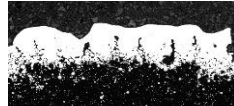
Scanning Speeds (mm/min)	Hatch distance, μm			
	50	75	100	125
150	 $E_s = 320.00 \text{ J/mm}^2$	 $E_s = 213.33 \text{ J/mm}^2$	 $E_s = 160.00 \text{ J/mm}^2$	 $E_s = 128.00 \text{ J/mm}^2$
300	 $E_s = 160.00 \text{ J/mm}^2$	 $E_s = 106.67 \text{ J/mm}^2$	 $E_s = 80.00 \text{ J/mm}^2$	 $E_s = 64.00 \text{ J/mm}^2$
1800	 $E_s = 26.67 \text{ J/mm}^2$	 $E_s = 17.78 \text{ J/mm}^2$	 $E_s = 13.33 \text{ J/mm}^2$	 $E_s = 10.67 \text{ J/mm}^2$
2100	 $E_s = 22.86 \text{ J/mm}^2$	 $E_s = 15.24 \text{ J/mm}^2$	 $E_s = 11.43 \text{ J/mm}^2$	 $E_s = 9.14 \text{ J/mm}^2$

Figure 11. Optical microscopy images from cross-section of single layer Cu10Sn samples produced with a laser power of 40W for different scanning speeds and hatch distances.

It is clearly seen that as the speed value increases, the melt pool depth value generally decreases and flattens for different hatch distance values. In other words, as the surface energy density values decrease, top surfaces of the sample improve. Thus, as the material surfaces flatter, a favorable environment is provided so that it can melt smoothly with the next layer without creating any pores. As can be seen from the Figure 11, the best surface images were seen in samples with a speed of 2100 mm/min. On the other hand, due to the lack of mobility of the gantry system used in this study, on which the blue lasers are located, the value of 2100

mm/min could not be exceeded. It is foreseen that balling defects may occur at scanning speeds above 2100 mm/min, as it cannot melt enough material. It is predicted that balling defects may occur, similar to the literature [29], since it cannot melt sufficient material at scanning speeds above 2100 mm/min. On the other hand, the laser power was reduced from 40 W to 20 W to examine the effects of laser power on the melt pool depth of the materials. In other words, the surface energy density value has been reduced by half. Figure 12 shows some selected optical microscopy images from cross-sections of single layer Cu10Sn samples produced with a laser power of 40W and 20W for different scanning speeds and hatch distances. Similar to Figure 11, Figure 12 clearly shows that lower surface energy density generally results in flatter material surfaces.

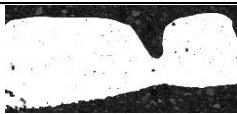
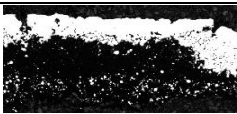
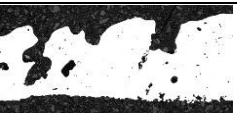
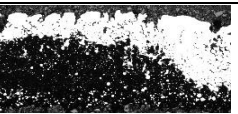

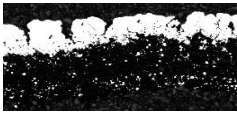


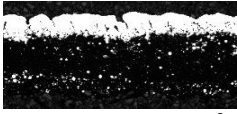
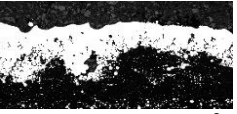

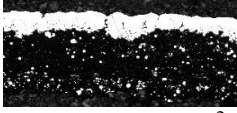
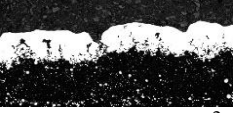
Scanning Speeds (mm/min)	Hatch distance, μm			
	50		75	
	Laser (W)		Laser (W)	
	40	20	40	20
150	 $E_s = 320.00 \text{ J/mm}^2$	 $E_s = 160.00 \text{ J/mm}^2$	 $E_s = 213.33 \text{ J/mm}^2$	 $E_s = 106.67 \text{ J/mm}^2$
	300	 $E_s = 160.00 \text{ J/mm}^2$	 $E_s = 80.00 \text{ J/mm}^2$	 $E_s = 106.67 \text{ J/mm}^2$
1800		 $E_s = 26.67 \text{ J/mm}^2$	 $E_s = 13.33 \text{ J/mm}^2$	 $E_s = 17.78 \text{ J/mm}^2$
	2100	 $E_s = 22.86 \text{ J/mm}^2$	 $E_s = 11.43 \text{ J/mm}^2$	 $E_s = 15.24 \text{ J/mm}^2$

Figure 12. Optical microscopy image comparison from cross-section of single layer Cu10Sn samples produced with a laser power of 40W and 20 W for different scanning speeds and hatch distances.

4. Conclusion

This study explores the potential of using 450 nm wavelength diode lasers to produce single-layer Cu10Sn samples. By systematically varying hatch distances (50, 75, 100, and 125 μm), scanning speeds (150 to 2100 mm/min), and laser powers (20 and 40 W), it was determined that the optimal parameters for enhancing sample quality. The investigation focused on surface roughness, relative density, and melt pool characterization, providing a comprehensive understanding of the samples' mechanical and physical properties. The findings revealed that samples produced with a 20 W laser power at low hatch distances and low scanning speeds (i.e., in high surface energy values) had surface roughness values up to 3.5 times lower than those produced with a 40 W laser power. Additionally, the highest relative density value of 87.84% was achieved with a 40 W laser power, a 50 μm hatch distance, and a scanning speed of 2100 mm/min. Furthermore, as a result of optical analysis taken from top

surface images, it was found that the surface energy density values of Cu₁₀Sn samples with a relative density value of 85% and above were in the range of 22–30 J/mm².

These findings validate the suitability of 450 nm diode lasers for Cu₁₀Sn sample production and offer a detailed framework for optimizing laser-based manufacturing processes, contributing significantly to the field of materials engineering.

Acknowledgment

This study was completed with support from the Turkish Government Ministry of Education, TUBITAK-2219 postdoctoral fellowship support program with project number 1059B192300923 and UK Research and Innovation, Engineering and Physical Sciences Research Council Grant EP/W024764/1.

REFERENCES

- [1] M. Khorasani, I. Gibson, A.H. Ghasemi, E. Hadavi, B. Rolfe, Laser subtractive and laser powder bed fusion of metals: review of process and production features, *Rapid Prototyp J* 29 (2023) 935–958. <https://doi.org/10.1108/RPJ-03-2021-0055>.
- [2] N. Huang, O.J. Cook, A.P. Argüelles, A.M. Beese, Review of Process–Structure–Property Relationships in Metals Fabricated Using Binder Jet Additive Manufacturing, *Metallography, Microstructure, and Analysis* 12 (2023) 883–905. <https://doi.org/10.1007/s13632-023-00998-4>.
- [3] O. Bouzaglou, O. Golan, N. Lachman, Process Design and Parameters Interaction in Material Extrusion 3D Printing: A Review, *Polymers (Basel)* 15 (2023) 2280. <https://doi.org/10.3390/polym15102280>.
- [4] S.K. Paral, D.-Z. Lin, Y.-L. Cheng, S.-C. Lin, J.-Y. Jeng, A Review of Critical Issues in High-Speed Vat Photopolymerization, *Polymers (Basel)* 15 (2023) 2716. <https://doi.org/10.3390/polym15122716>.
- [5] V.V.K. Doddapaneni, K. Lee, H.E. Aysal, B.K. Paul, S. Pasebani, K.A. Sierros, C.E. Okwudire, C. Chang, A Review on Progress, Challenges, and Prospects of Material Jetting of Copper and Tungsten, *Nanomaterials* 13 (2023) 2303. <https://doi.org/10.3390/nano13162303>.
- [6] T. Zhao, Z. Yan, B. Zhang, P. Zhang, R. Pan, T. Yuan, J. Xiao, F. Jiang, H. Wei, S. Lin, S. Chen, A comprehensive review of process planning and trajectory optimization in arc-based directed energy deposition, *J Manuf Process* 119 (2024) 235–254. <https://doi.org/10.1016/j.jmapro.2024.03.093>.
- [7] D. Dev Singh, T. Mahender, A. Raji Reddy, Powder bed fusion process: A brief review, *Mater Today Proc* 46 (2021) 350–355. <https://doi.org/10.1016/j.matpr.2020.08.415>.
- [8] S.R. Narasimharaju, W. Zeng, T.L. See, Z. Zhu, P. Scott, X. Jiang, S. Lou, A comprehensive review on laser powder bed fusion of steels: Processing, microstructure, defects and control methods, mechanical properties, current challenges and future trends, *J Manuf Process* 75 (2022) 375–414. <https://doi.org/10.1016/j.jmapro.2021.12.033>.

- [9] D. Buchbinder, H. Schleifenbaum, S. Heidrich, W. Meiners, J. Bültmann, High Power Selective Laser Melting (HP SLM) of Aluminum Parts, *Phys Procedia* 12 (2011) 271–278. <https://doi.org/10.1016/j.phpro.2011.03.035>.
- [10] T. Heeling, K. Wegener, The effect of multi-beam strategies on selective laser melting of stainless steel 316L, *Addit Manuf* 22 (2018) 334–342. <https://doi.org/10.1016/j.addma.2018.05.026>.
- [11] R.E. Gite, V.D. Wakchaure, A review on process parameters, microstructure and mechanical properties of additively manufactured AlSi10Mg alloy, *Mater Today Proc* 72 (2023) 966–986. <https://doi.org/10.1016/j.matpr.2022.09.100>.
- [12] S. Liu, Y.C. Shin, Additive manufacturing of Ti6Al4V alloy: A review, *Mater Des* 164 (2019) 107552. <https://doi.org/10.1016/j.matdes.2018.107552>.
- [13] M. Hoffmann, A. Elwany, Material extrusion additive manufacturing of AISI 316L pastes, *J Manuf Process* 108 (2023) 238–251. <https://doi.org/10.1016/j.jmapro.2023.10.078>.
- [14] S.S. Babu, N. Raghavan, J. Raplee, S.J. Foster, C. Frederick, M. Haines, R. Dinwiddie, M.K. Kirka, A. Plotkowski, Y. Lee, R.R. Dehoff, Additive Manufacturing of Nickel Superalloys: Opportunities for Innovation and Challenges Related to Qualification, *Metallurgical and Materials Transactions A* 49 (2018) 3764–3780. <https://doi.org/10.1007/s11661-018-4702-4>.
- [15] Q. Jiang, P. Zhang, Z. Yu, H. Shi, D. Wu, H. Yan, X. Ye, Q. Lu, Y. Tian, A Review on Additive Manufacturing of Pure Copper, *Coatings* 11 (2021) 740. <https://doi.org/10.3390/coatings11060740>.
- [16] D. Oropeza, T. Seager, S. Firdosy, J. Guerra, K. Billings, J.-P. Jones, D.C. Hofmann, S. Roberts, Porosity control of copper-based alloys via powder bed fusion additive manufacturing for spacecraft applications, *Journal of Porous Materials* 31 (2024) 779–791. <https://doi.org/10.1007/s10934-023-01544-x>.
- [17] Y. Liu, J. Zhang, Q. Tan, Y. Yin, S. Liu, M. Li, M. Li, Q. Liu, Y. Zhou, T. Wu, F. Wang, M.-X. Zhang, Additive manufacturing of high strength copper alloy with heterogeneous grain structure through laser powder bed fusion, *Acta Mater* 220 (2021) 117311. <https://doi.org/10.1016/j.actamat.2021.117311>.
- [18] T.-T. Ikeshoji, K. Nakamura, M. Yonehara, K. Imai, H. Kyogoku, Selective Laser Melting of Pure Copper, *JOM* 70 (2018) 396–400. <https://doi.org/10.1007/s11837-017-2695-x>.
- [19] M. Malý, D. Koutný, L. Pantělejev, L. Pambaguian, D. Paloušek, Effect of high-temperature preheating on pure copper thick-walled samples processed by laser powder bed fusion, *J Manuf Process* 73 (2022) 924–938. <https://doi.org/10.1016/j.jmapro.2021.11.035>.
- [20] M. Colopi, A.G. Demir, L. Caprio, B. Previtali, Limits and solutions in processing pure Cu via selective laser melting using a high-power single-mode fiber laser, *The International Journal of Advanced Manufacturing Technology* 104 (2019) 2473–2486. <https://doi.org/10.1007/s00170-019-04015-3>.

- [21] A. Hess, R. Schuster, A. Heider, R. Weber, T. Graf, Continuous Wave Laser Welding of Copper with Combined Beams at Wavelengths of 1030 nm and of 515 nm, *Phys Procedia* 12 (2011) 88–94. <https://doi.org/10.1016/j.phpro.2011.03.012>.
- [22] J.-M. Pelaprat, M. Finuf, R. Fritz, M. Zediker, Seeing Things in a New Light, *Laser Technik Journal* 15 (2018) 39–41. <https://doi.org/10.1002/latj.201800028>.
- [23] S. Engler, R. Ramsayer, R. Poprawe, Process Studies on Laser Welding of Copper with Brilliant Green and Infrared Lasers, *Phys Procedia* 12 (2011) 339–346. <https://doi.org/10.1016/j.phpro.2011.03.142>.
- [24] M. Haubold, A. Ganser, T. Eder, M.F. Zäh, Laser welding of copper using a high power disc laser at green wavelength, *Procedia CIRP* 74 (2018) 446–449. <https://doi.org/10.1016/j.procir.2018.08.161>.
- [25] T. Shibata, M. Tsukamoto, Y. Sato, S.-I. Masuno, Effect of input energy on densification for pure copper fabricated by SLM with blue diode laser, in: H. Helvajian, B. Gu, H. Chen (Eds.), *Laser 3D Manufacturing VI*, SPIE, 2019: p. 34. <https://doi.org/10.1117/12.2509459>.
- [26] E. Hori, Y. Sato, T. Shibata, K. Tojo, M. Tsukamoto, Development of SLM process using 200 W blue diode laser for pure copper additive manufacturing of high density structure, *J Laser Appl* 33 (2021). <https://doi.org/10.2351/7.0000311>.
- [27] M. Alsaddah, A. Khan, K. Groom, K. Mumtaz, Use of 450-808 nm diode lasers for efficient energy absorption during powder bed fusion of Ti6Al4V, *The International Journal of Advanced Manufacturing Technology* 113 (2021) 2461–2480. <https://doi.org/10.1007/s00170-021-06774-4>.
- [28] C. Wei, Z. Sun, Y. Huang, L. Li, Embedding anti-counterfeiting features in metallic components via multiple material additive manufacturing, *Addit Manuf* 24 (2018) 1–12. <https://doi.org/10.1016/j.addma.2018.09.003>.
- [29] L. Zhang, H. Attar, M. Calin, J. Eckert, L. Zhang, H. Attar, M. Calin, J. Eckert, Review on manufacture by selective laser melting and properties of titanium based materials for biomedical applications, *Materials Technology* 7857 (2016) 1–9. <https://doi.org/10.1179/1753555715Y.0000000076>.